Aerial 360-Degree Video Delivery for Immersive First Person View UAV Navigation

Simran Singh, Jacob Chakareski
Dept. of Informatics, New Jersey Institute of Technology, Newark, NJ, USA

2023 IEEE International Symposium on Multimedia (ISM) | 979-8-3503-9576-1/23/$31.00 ©2023 IEEE | DOI: 10.1109/ISM59092.2023.00026

***Abstract*—Adaptive transmission of conventional video from a UAV to the ground has been researched for various applications, but the research topic of 360° video transmission from a UAV for the specific application of first-person view (FPV) based navigation is still nascent. In this work, we present adaptive 360° video compression and streaming methods to optimize the perceptual quality of experience of a pilot, who navigates the UAV in real time by viewing this immersive FPV feed, which is sent wirelessly from the UAV to the pilot. This adaptation of the 360° FPV feed is performed in response to the wireless channel conditions and the pilot's viewport, wherein each 360° frame is split into two regions of variable size, one meant to be within the pilot's viewport and the other outside. Each region is encoded using different H.265 quantization parameters (QP) and modulation orders. We model the scenario realistically by generating probability distributions of the variation in frame size and quality with QP, for aerial 360° videos. These models are expressed using a two-term exponential function, whose parameters are also provided. This model achieves lower prediction errors than the single-term exponential and power law functions. Simulations on a set of aerial 360-degree videos demonstrate that the adaptive approach achieves 9.73 dB (21.77%) greater QoE than a baseline approach that utilizes throughput-based adaptive bit rate algorithm (ABR) to tune QP per GoP, and a 5G new radio adaptive modulation scheme (AMS) to tune modulation order. Additionally, we present a deep reinforcement learning approach to adapt FPV, which achieves an expected pilot QoE just 2.07 dB lower than the adaptive approach, while being significantly faster and requiring no prior knowledge of the environment.**

***Index Terms*—360-degree video, quality of experience, first-person view, UAVs, wireless communications**

I. Introduction

UAV video applications can benefit greatly from 360° video technology, which provides a more immersive experience than conventional cameras. An on-board 360° camera on a UAV enables the ground pilot to conveniently scan the UAV's surroundings simply by changing the viewing direction within the head-mounted display (HMD) without changing the UAV's course, similar to how drivers check their surroundings when driving a car. This enhanced situational awareness can enhance first-person view (FPV) applications, wherein pilot on the ground navigates a UAV by viewing the video provided by the UAV's on-board camera. FPV applications include search and rescue missions to locate survivors, aerial surveillance to monitor crowds or infrastructure, or for aerial videography to cover live events.

The Insta360 Sphere camera [1] integrates with DJI Air 2 and Air 2S such that the drone itself does not appear in the captured frames, resulting in a truly flying 360° camera. Commercial 360° cameras are designed to save video frames locally, with limited live-streaming capabilities. Streaming over the air, for real-time applications has its unique challenges. UAV motion may result in rapid changes in the wireless channel quality, in response to which the encoded video quality and the radio modulation and coding must be tuned to ensure that the frames are delivered both reliably and with sufficient quality. An FPV downlink feed also needs to be adapted such that the portion of the 360° video within the pilot's continuously changing viewport is of sufficient quality, where the viewport is the region of the HMD currently being viewed by the pilot.

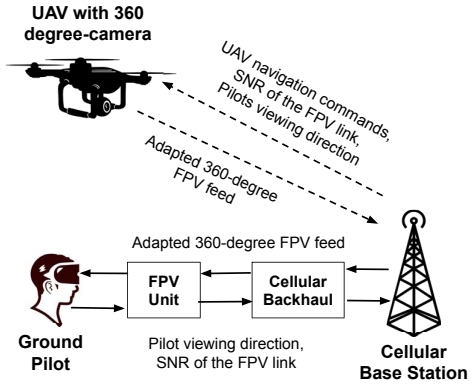

Fig. 1. Scenario under consideration: Adaptation of a 360° FPV downlink from a UAV to a ground pilot.

Various aspects of drone-based 360° video transmission have been studied, such as the suitability of the WebRTC transport protocol [2], resource (time, frequency, compute) allocation to optimize the quality of experience (QoE) of ground users [3]–[8], and the impact of region of interest coding on pilot QoE [9] in low-bandwidth networks. Viewport adaptive 360° transmission has also been studied extensively [10]–[12], however, for the general Internet, rather than for UAV navigation applications. To the best of our knowledge, viewport-adaptive techniques have not been studied in detail for the scenario of 360° transmission from a UAV to a ground pilot, taking into account the pilot head movements and changes in the wireless air to ground communication channel, for real-time UAV navigation. We address this gap as follows.

We theoretically model the scenario of 360° video transmission from a UAV for FPV-based navigation, taking into account UAV motion, the pilot's viewing pattern and field of vision, rate-distortion characteristics of aerial 360° video, and stochastic wireless channel characteristics. Each 360° frame captured at the UAV, is split into two regions, one predicted to

This work has been supported in part by the NSF under awards CCF-2031881, ECCS-2032387, CNS-2040088, CNS-2032033, and CNS-2106150, by the NIH under award R01EY030470, and by the Panasonic Chair of Sustainability at NJIT.

979-8-3503-9576-1/23/$31.00 ©2023 IEEE
DOI 10.1109/ISM59092.2023.00026

be within the pilot's field of view and the other outside. These two regions are then encoded using distinct QP values and modulation orders, to maximize the instantaneous visual quality of the pilot, while satisfying constraints on the reliability of the communication link, expressed in terms of probability of frame reception, and on the latency of the FPV feed. We compare the performance of various approaches: simple exhaustive search, a solution based on deep reinforcement learning, and a baseline that tunes QP using throughput-based adaptive bit rate (ABR) and modulation order using 5G-NR adaptive modulation scheme (AMS). Additionally, we generate models for frame sizes and quality, obtained by encoding aerial videos using H.265 codec at various QP values, using a two-term exponential function.

II. Modelling 360° FPV Navigation

We consider a scenario as shown in Fig. 1, wherein a UAV, equipped with a 360° camera, transmits the FPV feed wirelessly to a pilot on the ground. The pilot views this FPV feed in real-time on the HMD and navigates the UAV. The pilot's viewing direction and the signal to noise ratio (SNR) of the wireless FPV link is fed back to the UAV continuously. Using this feedback, the UAV adapts the 360° FPV feed to maximize the instantaneous QoE within the pilot's viewport. We assume a constant frame resolution of h_{Fr} horizontal and v_{Fr} vertical pixels, and a a target frame rate of f_{Fr}.

A. Wireless Connectivity

Wireless connectivity is provided by N_{B} cellular base stations (BSs) operating at millimeter (mmWave) frequencies, each of which transmits at P_{B} watts. For simplicity, we assume that the UAV travels in a straight line between a start and end waypoint, denoted as $\mathbf{X}_{\mathrm{U,S}}$ and $\mathbf{X}_{\mathrm{U,E}}$, at a constant velocity of v m/s. $\mathbf{X}_{i,\mathrm{B}}$ denotes the position of the i^{th} BS, and $\mathbf{X}_{\mathrm{U}}(t)$ denotes the UAV's position at time t. The distance between the UAV and the i^{th} BS, denoted as $d_{\mathrm{i}}(t)$ is:

$$d_{\mathrm{i}}(t) = |\mathbf{X}_{\mathrm{U}}(t) - \mathbf{X}_{i,\mathrm{B}}|^2. \tag{1}$$

We compute the probability of line of sight (LoS) between the UAV and i^{th} BS, denoted as $\mathbb{P}_{\mathrm{LoS,i}}(t)$, using a 3GPP model:

$$\mathbb{P}_{\mathrm{LoS,i}}(t) = \begin{cases} 1, & \ell_{\mathrm{2D}} < k_1(t), \\ \frac{k_1(t)}{\ell_{\mathrm{2D}}(t)} + (1 - \frac{k_1(t)}{\ell_{\mathrm{2D}}(t)})e^{\frac{-\ell_{\mathrm{2D}}(t)}{k_2(t)}}, & \ell_{\mathrm{2D}} > k_1(t), \end{cases}$$

where $\ell_{\mathrm{2D}}(t)$ is the two-dimensional (2D) distance between the UAV at time t and the i^{th} BS, and $k_1(t)$ and $k_2(t)$ are functions of the height of the UAV at time t. The path loss between the UAV and the i^{th} BS, denoted as $p_i(t)$, is calculated as [13]:

$$\begin{aligned} \rho_i(t) =& 32.4 - 180\log_{10}(f_{\mathrm{c}}) + 10A\big(h_{\mathrm{U}}(t)\big)^B\log_{10}(d_i(t)\big) \\ &+ \mathcal{N}(0, \sigma_{\mathrm{N}}), \end{aligned} \tag{2}$$

where f_{c} is the transmission frequency, and $h_{\mathrm{U}}(t)$ is the height of the UAV at time t. σ_{N} is the standard deviation of the Gaussian-distributed shadow fading, and depends on the environment, e.g. urban vs suburban. A and B are parameters that depend on the environment and the presence of an LoS path between the UAV and the BS, as calculated in (2). The signal strength at the UAV from the i^{th} BS is calculated as:

$$s_i(t) = \rho_i(t)P_{\mathrm{B}}. \tag{3}$$

At any given time t, the UAV associates with the BS that has the strongest received signal strength. The SNR of the FPV link, denoted as $\gamma(t)$, is then calculated as:

$$\gamma(t) = \frac{\big(\max_i\ \rho_i(t)\big)P_{\mathrm{U}}}{BN_o}, \tag{4}$$

where N_o is the noise spectral density, B is the transmission bandwidth, and P_{U} is the UAV transmission power.

B. Pilot's Viewing Model

At time t, let the heading angle of the UAV be denoted by the pair of horizontal and vertical angles: $\{\theta_{\mathrm{U}}(t), \phi_{\mathrm{U}}(t)\}$. The pilot's viewing direction is similarly represented by the pair: $\{\theta_{\mathrm{P}}(t), \phi_{\mathrm{P}}(t)\}$. A study on the head movements of pilots [14] found that pilots pre-dominantly viewed along the aircraft heading direction. Pilots had symmetric head movements along the horizontal plane and slightly skewed head movements in the vertical plane, where pilots tend to look down (towards south) more than up (towards north). Accordingly, we assume a pilot viewing model as follows.

As shown in Fig. 2, the pilot is assumed to constantly scan around the UAV's heading angle, between θ_{H} degrees east and west, and vertically between $\phi_{\mathrm{N}} \in [0, \frac{\pi}{2}]$ (towards north) and $\phi_{\mathrm{S}} \in [\frac{-\pi}{2}, 0]$ (towards south). We assume that $|\phi_{\mathrm{S}}| > \phi_{\mathrm{N}}$, i.e. the pilot scans down towards south more than up towards north. The horizontal viewing direction is assumed to be a normal distribution with its mean along the UAV heading direction, such that the 95% confidence interval is within a deviation θ_{H} from the mean. Mathematically,

$$\theta_{\mathrm{P}}(t) = \mathcal{N}\big(\theta_{\mathrm{U}}(t), \frac{\theta_{\mathrm{H}}}{1.96}\big), \tag{5}$$

using the property that, in a normal distribution, 95% of all values lie within 1.96 standard deviation of the mean.

In the vertical plane, the pilot views along the UAV heading direction with a probability p_ϕ, and deviates with a probability $1 - p_\phi$, in which case the vertical viewing angle is uniformly distributed between ϕ_{N} and ϕ_{S}, around $\phi_{\mathrm{U}}(t)$, as:

$$\phi_{\mathrm{P}}(t) = \begin{cases} \phi_{\mathrm{U}}(t), \text{with probability } p_\phi \\ \\ \mathcal{N}(\phi_{\mathrm{U}}(t) + \frac{\phi_{\mathrm{N}}+\phi_{\mathrm{S}}}{2}, \frac{|\phi_{\mathrm{N}}-\phi_{\mathrm{S}}|}{3.92}), \\ \text{with probability } 1 - p_\phi \end{cases} \tag{6}$$

C. Viewport Adaptive Video Encoding

Let t denote the time instant at which the UAV is about to encode the captured 360° panorama. Based on the knowledge of the pilot's viewing angle $\{\theta_{\mathrm{P}}(t), \phi_{\mathrm{P}}(t)\}$, the FPV system at the UAV partitions the sphere into two regions, one meant to be within the pilot's viewport and other outside. This partitioning is performed on the basis of two horizontal and two vertical angles: $\theta'_{\mathrm{H}}(t)$ east, $\theta'_{\mathrm{H}}(t)$ west, $\phi'_{\mathrm{N}}(t)$ north, and $\phi'_{\mathrm{S}}(t)$ south. We assume equi-rectangular projection, wherein constant increments in the horizontal and vertical angles in the

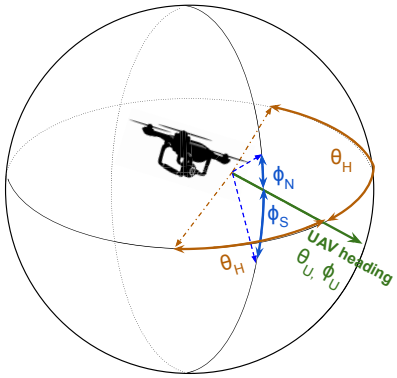

Fig. 2. Selecting a region of interest from the 360° viewport based on the UAV heading, $\theta_{\rm H}$, $\phi_{\rm S}$, and $\phi_{\rm N}$.

spherical plane correspond to constant increments along the x and y axes in the two dimensional (2-D) Cartesian plane. After equi-rectangular projection, let there be $p_{\rm I}(t)$ pixels inside the viewport and $p_{\rm O}(t)$ pixels outside the viewport:

$$p_{\rm I}(t) = \frac{h_{\rm Fr}\theta'_H}{180^\circ} \times \frac{v_{\rm Fr}(\phi'_N + |\phi'_S|)}{360^\circ} \qquad (7)$$
$$p_{\rm O}(t) = h_{\rm Fr}v_{\rm Fr} - p_{\rm I}(t)$$

For the assumed pilot viewing model, if $\theta'_{\rm H}(t) = \theta_{\rm H}$, $\phi'_{\rm N}(t) = \phi_{\rm N}$, and $\phi'_{\rm S}(t) = \phi_{\rm S}(t)$, then there is 95% probability that the viewport chosen by the FPV system contains the pilot's viewing direction.

The region within the viewport chosen by the FPV system is encoded using H.265 codec at a QP of $q_{\rm I}(t)$, while the region outside at $q_{\rm O}(t)$. The size of the encoded frame, and its quality, measured in peak signal-to-noise ratio (PSNR), both depend on the QP. For the frame encoded at a QP of q, we use $\mathcal{F}_{\rm FrSz}(q)$ to denote the cumulative distribution function (CDF) of the encoded frame size, and $\mathcal{F}_{\rm FrQ}(q)$ to denote the CDF of the encoded frame quality. We derived these CDFs for aerial 360° videos by compressing videos from [15] using H.265 at various QP values (10 to 50 in steps of 5), for a constant group of pictures (GOP) size of 50. Bipredictive frames (B-frames) were disabled and videos were downloaded in either 4K or 8K resolution. The list of evaluated videos is in Table I, and their Youtube URLs are shared in the Appendix. For each video set and at each QP value, we measured the frame size and PSNR of each resultant encoded frame. The variation in frame size and frame quality with QP was modelled as an exponential function of the form $y = a * {\rm e}^{-bx} + c * {\rm e}^{-dx}$, different from the single-term exponential and power law functions used to model rate-distortion characteristics in [16]. An intuitive understanding is presented as follows.

Fig. 3 shows the CDF of encoded frame sizes for various QP values, for aerial 360° videos of Chicago and Huangshan (a mountain range in Eastern China). The distribution is similar at higher QP, implying that both videos have similar compression characteristics. At lower QPs, the distibutions begin to vary slightly, though the mean values are similar. Fig. 4 shows the CDF of PSNR values of the luminance (Y) component as a function of QP. Both locations have similar PSNR values, as the QP is increased from 5 to 25. At lower QP values, the

TABLE I
DATASET OF EVALUATED AERIAL 360° VIDEOS

Location	Resolution	Frame Rate	Environment
Chicago	7680x3840	30	Urban
Lucerne	3840x2048	24	Urban
San Francisco	7680x3840	30	Urban
Zurich	3840x2048	30	Urban
Bryansk Forest	7680x3840	30	Nature
Hawaii	7680x3840	30	Nature
Huangshan	7680x3840	50	Nature
Lake Hibara	7680x3840	30	Nature

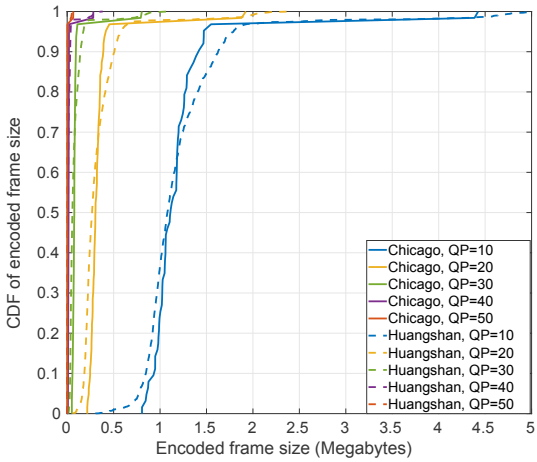

Fig. 3. CDF of encoded frame sizes for various QP values, for aerial 360° videos of Chicago and Lake Hibara.

PSNR of Huagshan is marginally higher, and the difference reduces at higher QPs. The similarity in video characteristics can be explained by considering that, at the high altitude from which the UAV captures the video scene, majority of the scene is static, and the compression statistics are thus similar. The rate-distortion characteristics of all videos is shown in Fig. 5.

Using this dataset, we generate the distribution of frame sizes specifically for key frames (I-frames) and non-key frames (B-frames and P-frames). Such granular distributions are useful when considering the real-time latency constraints involved in FPV navigation, i.e. depending on the GoP size, the current frame is classified as a key or a non-key frame and the corresponding frame-size distribution is used. We use $b_{\rm I}(t)$ to denote the number of bits used to represent the region inside the viewport encoded at a QP $q_{\rm I}(t)$, and $b_{\rm O}(t)$ for the number of bits outside the viewport, encoded at $q_{\rm O}(t)$. $b_{\rm I}(t)$ and $b_{\rm O}(t)$ are both random variables, whose distribution can be obtained from $\mathcal{F}_{\rm FrSz}(q)$.

D. Video Transmission and Reception

We assume that a modulation order of $m_{\rm I}(t)$ is used for the region within the viewport and $m_{\rm O}(t)$ for the region outside the viewport. For signal bandwidth of B Hz, the symbol rate is $\frac{B}{2}$, and the transmission bit rate is:

$$r_{\rm I}(t) = \frac{B\log_2\left(m_{\rm I}(t)\right)}{2}, \quad r_{\rm O}(t) = \frac{B\log_2\left(m_{\rm O}(t)\right)}{2}. \qquad (8)$$

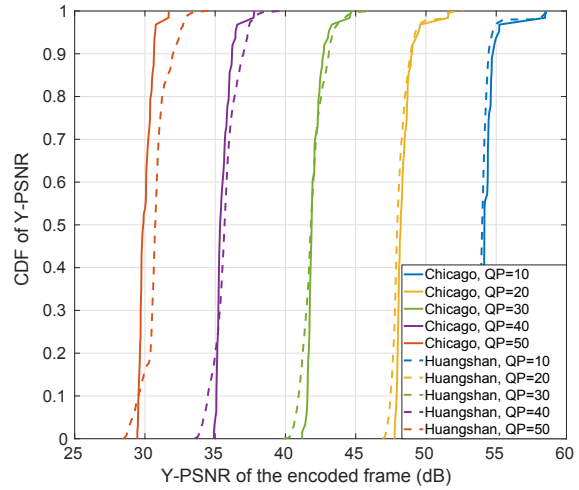

Fig. 4. CDF of the PSNR of the encoded frame, for various QP values, for aerial 360° videos of Chicago and Lake Hibara.

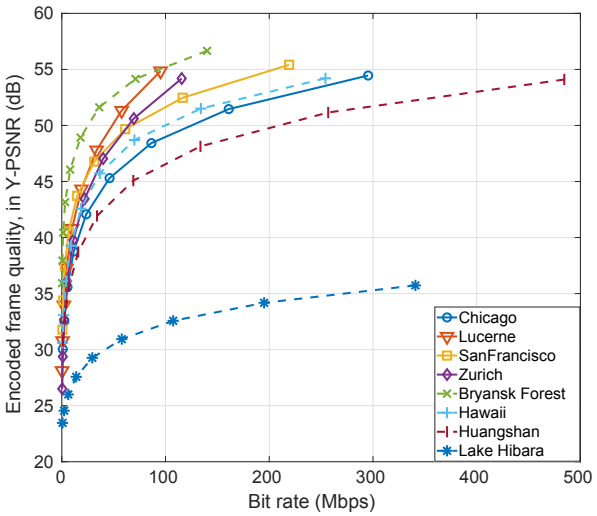

Fig. 5. Average encoded video quality, measured in PSNR (dB), vs. average encoded video bit rate (Mbps), for all considered aerial 360° videos.

The propagation delay of the encoded frame from the UAV to the associated BS, denoted as $T_{\mathrm{P}}(t)$ is calculated as:

$$T_{\mathrm{P}}(t) = \frac{d_{\mathrm{BS}}(t)}{c}, \tag{9}$$

where c is the speed of light and $d_{\mathrm{BS}}(t)$ is the distance of the UAV from its associated BS. The networking delay encountered by the encoded frame as it is forwarded from the BS to the pilot is denoted as T_{N}. For simplicity, we assume that the communication link between the BS and the pilot has sufficient capacity and thus, T_{N} is constant. We define frame latency, denoted as $T_{\mathrm{FrL}}(t)$ as the time interval between the instant at which the frame is captured at the UAV and the instant at which it is displayed to the pilot:

$$T_{\mathrm{FrL}}(t) = T_{\mathrm{Enc}}(t) + \frac{1}{r_{\mathrm{C}}}\left(\frac{b_{\mathrm{I}}(t)}{r_{\mathrm{I}}(t)} + \frac{b_{\mathrm{O}}(t)}{r_{\mathrm{O}}(t)}\right) + T_{\mathrm{N}} + T_{\mathrm{P}}(t), \tag{10}$$

where r_{C} is the channel coding rate and $T_{\mathrm{Enc}}(t)$ denotes the time required to encode the frame:

$$T_{\mathrm{Enc}}(t) = \frac{p_{\mathrm{I}}(t)}{p(t)} T_{\mathrm{Enc}}(q_{\mathrm{I}}(t)) + \frac{p_{\mathrm{O}}(t)}{p(t)} T_{\mathrm{Enc}}(q_{\mathrm{O}}(t)). \tag{11}$$

Expected encode time duration, as a function of QP, measured during the encoding process, are used to calculate (11). Since $b_{\mathrm{I}}(t)$ and $b_{\mathrm{O}}(t)$ are random variables, $T_{\mathrm{FrL}}(t)$ is also a random variable. Let the probability distribution of T_{FrL} be denoted as $\mathbb{P}_{\mathrm{FrL}}(t)$. Then, the expected frame latency is calculated as:

$$\mathbb{E}_{\mathrm{FrL}}(t) = \int \tau \mathbb{P}_{\mathrm{FrL}}(T_{\mathrm{FrL}} = \tau) d\tau, \tag{12}$$

where τ denotes the domain of the frame latency values, over which its expected value is calculated. We utilize LDPC channel coding, as also used in 5G NR. The variation in bit error rate, as a function of the given LDPC coding rate and the modulation scheme, has been presented in literature [17]. For simplicity, we assume that all bits of the encoded frame must be successfully received at the receiver for successful decoding. Additionally, for non-key frames, the previous predictor frame must also be successfully received. Accordingly, for non-key frames, the probability that the frame is successfully received, denoted as $\mathbb{P}_{\mathrm{FrRx}}(t)$ is calculated as follows:

$$\mathbb{P}_{\mathrm{FrRx}}(t) = (1 - e_{\mathrm{I}}(t))^{b_{\mathrm{I}}(t)} (1 - e_{\mathrm{O}}(t))^{b_{\mathrm{O}}(t)} \mathbb{P}_{\mathrm{FrRx}}(t - T_{\mathrm{FrL}}).$$

Independent receipt probabilities are assumed for key frames.

E. Quality of Experience (QoE) Metric

The human visual span can be categorized into three regions, based on the used the distribution of retinal cones [18]. The most detailed is the foveal region, with a radius of 1° around the viewing direction. The second region, termed the central region, has a span of 30° around the viewing direction. This region provides visual information and location of most objects in the line of sight, while the region outside 30°, termed the peripheral region, provides general awareness of larger objects and motion cues. Accordingly, we define the QoE of the pilot, denoted as $\mathcal{Q}_{\mathrm{P}}(t)$, as follows:

$$\mathcal{Q}_{\mathrm{P}}(t) = W_{\mathrm{C}} \mathcal{Q}_{\mathrm{Fr,C}}(t) + W_{\mathrm{P}} Q_{\mathrm{Fr,P}}(t) + W_{\mathrm{NP}} \mathcal{Q}_{\mathrm{Fr,NP}}(t),$$

where $\mathcal{Q}_{\mathrm{Fr,C}}(t)$, $\mathcal{Q}_{\mathrm{Fr,P}}(t)$, and $\mathcal{Q}_{\mathrm{Fr,NP}}(t)$ denote the quality of the encoded frame within the central region, within the peripheral region excluding the inner central region, and within the non-peripheral region of the pilot, respectively. $W_{\mathrm{C}}, W_{\mathrm{P}}$, and W_{NP} are weights assigned to these quality measures such that $W_{\mathrm{C}} > W_{\mathrm{P}} > W_{\mathrm{O}}$ encourages the FPV adaptation algorithm to prioritize maximizing the video

frame quality within the central region. The qualities $\mathcal{Q}_{\mathrm{Fr,C}}(t)$, $\mathcal{Q}_{\mathrm{Fr,P}}(t)$, and $\mathcal{Q}_{\mathrm{Fr,NP}}(t)$ are calculated as follows:

$$\begin{aligned}\mathcal{Q}_{\mathrm{Fr,C}}(t) =& \frac{|\mathcal{R}_{\mathrm{C}} \cap \mathcal{R}_{\mathrm{I}}(t)|}{|\mathcal{R}_{\mathrm{C}}|} q_{\mathrm{I}}(t) + \frac{|\mathcal{R}_{\mathrm{C}} \cap \mathcal{R}_{\mathrm{O}}(t)|}{|\mathcal{R}_{\mathrm{C}}|} q_{\mathrm{O}}(t),\\ \mathcal{Q}_{\mathrm{Fr,P}}(t) =& \frac{|(\mathcal{R}_{\mathrm{P}} - \mathcal{R}_{\mathrm{C}}) \cap \mathcal{R}_{\mathrm{I}}(t)|}{|(\mathcal{R}_{\mathrm{P}} - \mathcal{R}_{\mathrm{C}})|} q_{\mathrm{I}}(t) + \\ & \frac{|(\mathcal{R}_{\mathrm{P}} - \mathcal{R}_{\mathrm{C}}) \cap \mathcal{R}_{\mathrm{O}}(t)|}{|\mathcal{R}_{\mathrm{P}} - \mathcal{R}_{\mathrm{C}}|} q_{\mathrm{O}}(t),\\ \mathcal{Q}_{\mathrm{Fr,NP}}(t) =& \frac{|\mathcal{R}_{\mathrm{NP}} \cap \mathcal{R}_{\mathrm{I}}(t)|}{|\mathcal{R}_{\mathrm{C}}|} q_{\mathrm{I}}(t) + \frac{|\mathcal{R}_{\mathrm{NP}} \cap \mathcal{R}_{\mathrm{O}}(t)|}{|\mathcal{R}_{\mathrm{C}}|} q_{\mathrm{O}}(t),\end{aligned}$$

where $\mathcal{R}_{\mathrm{C}}$, $\mathcal{R}_{\mathrm{P}}$, $\mathcal{R}_{\mathrm{NP}}$, $\mathcal{R}_{\mathrm{I}}$, and $\mathcal{R}_{\mathrm{O}}$ denote the regions: central, peripheral, outside the peripheral, inside the estimated viewport, and outside the estimated viewport, respectively. The operator $|.|$ denotes the area of a region.

III. 360° FPV Adaptation

We define the FPV adaptation problem as a discrete-time decision process which takes place at the FPV system of the UAV. For each captured frame at time t, the UAV chooses the QP and modulation order for the regions within and outside the pilot's viewport, as known by the UAV at time t, to maximize the QoE of the pilot, subject to constraints on the frame latency and probability of frame reception. Mathematically,

$$\begin{aligned}\underbrace{\max}_{\substack{\theta'_H(t),\phi'_N(t),\phi'_S(t)\\ q_{\mathrm{I}}(t),q_{\mathrm{O}}(t),m_{\mathrm{I}}(t),m_{\mathrm{O}}(t)}} \quad & \mathcal{Q}_{\mathrm{P}}(t + T_{\mathrm{FrL}})\\ \text{such that: } & c_1 : \mathbb{E}\left(T_{\mathrm{FrL}}(t)\right) <= \frac{1}{f_{\mathrm{Fr}}}\\ & c_2 : \mathbb{P}_{\mathrm{FrRx}}(t) > \alpha\\ & c_3 : \theta'_H(t) \in \boldsymbol{\theta},\\ & c_4 : \phi'_N(t) \in \boldsymbol{\Phi}, \phi'_S(t) \in \boldsymbol{\Phi},\\ & c_5 : q_{\mathrm{I}}(t), q_{\mathrm{O}}(t) \in \mathbf{q},\\ & c_6 : m_{\mathrm{I}}(t), m_{\mathrm{O}}(t) \in \mathbf{m}, \end{aligned} \tag{13}$$

where α is the guarantee to be provided on the probability of frame reception and $\mathbb{E}\left(T_{\mathrm{FrL}}(t)\right)$ is the expected frame latency. $\boldsymbol{\theta}, \boldsymbol{\Phi}, \mathbf{q}, \mathbf{m}$ represent the search range for the horizontal viewport limit, vertical viewport limits, QPs, and modulation order. Constraint c_1 ensures that the expected frame latency matches the target bit rate requirement, while constraint c_2 guarantees successful frame reception. Constraints $c_3 - c_6$ capture the discrete optimization search space.

A. FPV Adaptation using Exhaustive Search

To solve this optimization problem, we iterate over all parameter combinations exhaustively to first prune combinations that disobey the constraints. From the combinations that remain, we choose those that maximize the QoE. In practice, computation delays can be minimized by storing these optimum parameters values as a function of channel SNR and pilot viewing direction as a look-up table on memory, or they may be provided by a trained neural network. Studies [14] have shown that a pilot's scanning rate does not exceed 120° per second. For simplicity, we assume $\mathcal{Q}_{\mathrm{P}}(t + T_{\mathrm{FrL}}) = \mathcal{Q}_{\mathrm{P}}(t)$ for the considered frame rates. For instance, the pilot's viewing angle will not change by more than approximately 4° between consecutive frames, at 30 frames per second. This optimization approach utilizes models of the variation in expected frame latency and frame size with QP, derived from the offline analysis of general aerial 360° videos, as presented in our supplementary data-set. Thus, the performance of the online optimization depends on the accuracy of the generated offline models. Exhaustive search is computationally expensive and its time complexity is: $\mathcal{O}(|\boldsymbol{\theta}|^2 \times |\boldsymbol{\Phi}|^2 \times |\mathbf{q}|^2 \times |\mathbf{m}|^2)$.

B. Deep Reinforcement Learning-Based FPV Adaptation

The applicability of the exhaustive search is limited to the environments for which its analytical models were derived. To adapt the 360° FPV feed in previously unseen environments, we also evaluate the use of a deep reinforcement learning (DRL) algorithm approach. DRL does not require such prior knowledge and learns the relationships the optimal parameter combinations through training. Unlike conventional reinforcement learning techniques, DRL approaches can handle large action and state spaces, since they use a neural network as a functional approximation of the Q-table, and they are not affected by the curse of dimensionality. While the training process of a deep RL agent is time-consuming, its deployment only requires a single forward pass through the neural network, such that it can handle dynamic environments and operate in real-time. The action set of the DRL agent is formed by the set of optimization parameters

$$a(t) = \{\theta'_H(t), \phi'_N(t), \phi'_S(t), q_{\mathrm{I}}(t), q_{\mathrm{O}}(t), m_{\mathrm{I}}(t), m_{\mathrm{O}}(t)\}, \tag{14}$$

the state set is formed by the instantaneous SNR and pilot viewing direction

$$s(t) = \{\gamma(t), \theta_{\mathrm{U}}(t), \phi_{\mathrm{U}}(t)\}, \tag{15}$$

while the reward function is the instantaneous QoE of the pilot, $\mathcal{Q}_{\mathrm{P}}(t)$, with negative rewards for actions that lead to constraints being violated. At time t, the reward of taking action a in state s at time is defined as follows:

$$r(s,a) = \begin{cases} \mathcal{Q}_{\mathrm{P}}(t), \text{if constraints are satisfied,} \\ -\infty, \text{if constraints are not satisfied} \end{cases} \tag{16}$$

The interaction of the reinforcement learning agent with the environment is shown in Fig. 6. Value-based DRL algorithms evaluate the value of each action at a given state and the optimal policy, termed as the Q value:

$$Q_n(s,a) \leftarrow (1-\eta) Q_n(s,a) + \eta \Big[r_n + \beta \max_a Q_n(s',a) \Big], \tag{17}$$

where η, the learning rate, is the agent's willingness to learn from the UAV FPV resource allocation environment, β is the discount factor, r_n is the reward at timestep n, and s' is the next state. The agent learns the Q function in the training phase, by exploring the impact of all possible QP and radio parameter combinations, in various states, i.e., at various channel SNRs and pilot viewing directions, on the pilot QoE. Once the Q function has been properly learned, the parameter

combination to maximize the QoE in a given state, is obtained by choosing the action with the highest Q value:

$$a^* = \arg\max_a \ Q(s,a). \tag{18}$$

We compare two DRL architectures: deep deterministic policy gradient (DDPG) and duelling deep queue learning (DDQN). DDQN uses a target and an online neural network. DDPG improves on DDQN by using two types of networks - an actor network and a critic network. The actor is responsible for learning the policy of choosing optimal actions in a given state, while the critic evaluates the actor's policy and gives feedback on the selected actions. The actor and critic networks, in turn, consist of a target and an online network. We utilized a neural network with an input layer (which receives the state set), a middle layer with 64 densely connected neurons (which functions as the intelligent optimizer), and an output layer (which yields the action set). The actor is parameterized by θ, such that $\pi_\theta(s)$ denotes a unique action policy. The critic is denoted by parameter ω, such that $Q^\omega(s,a)$ denotes the Q function approximator used by the critic to calculate the value of taking action a in state s. $Q^\pi(s,a)$ denotes the target Q function network used by the critic. The parameter w is chosen to minimize the mean square error as follows:

$$\epsilon(\omega) = \mathbb{E}_{s\sim\rho^\pi, a\sim\pi_\theta}\left[\left(Q^\omega(s,a) - Q^\pi(s,a)\right)^2\right] \tag{19}$$

The actor network is updated by taking the gradient of the expected return as follows:

$$\Delta_\theta J(\pi_\theta) = \mathbb{E}_{s\sim\rho^\pi, a\sim\pi_\theta}\left[\Delta_\theta \log \pi_\theta(a|s) Q^\omega(a,s)\right] \tag{20}$$

C. Baseline and Static Resource Allocation

The performance of our proposed approach is compared with a baseline approach, which utilizes a throughput-based ABR algorithm for video adaptation combined with 5G-NR AMS, proposed in [19], for modulation order selection. This baseline algorithm transmits only the portion of 360° feed within the pilot's viewport. The ground station (client) measures the received throughput over a GoP, and feeds this information back to the UAV (server). The FPV system at the UAV then uses a look-up table to select the optimum QP values for the next GoP to match the observed channel throughput. Three non-adaptive approaches were also evaluated, designed to cover representative strategies: 1) Maximize frame quality while using the lowest available modulation order, to ensure a low frame error rate, 2) Minimize frame quality while using the highest available modulation order, to ensure largest data rates and hence a low frame latency, and 3) A compromise between these two extremes, wherein intermediate values are chosen for QP and the modulation scheme.

IV. Simulation Results

A. Models of Frame Size and Frame Quality vs QP

As described in Section. II-C, we generate models for the variations in expected frame size and expected frame quality as a function of QP, using a two-term exponential function. The performance of this two-term exponential function was compared with two other models widely used to model rate distortion characteristics [16]: a single-term exponential function of the form $a * \mathrm{e}^{-b\mathrm{x}}$ and a single term power law function of the form $a * \mathrm{x}^b$. A two-term power law function, of the form $a * \mathrm{x}^b + c$, was also evaluated. The parameters of these prediction models are found using non-linear least squares curve fitting. Fig. 7 shows the absolute error in predicting Y-PSNR and frame size for the aerial 360° video of Chicago, illustrating that the two-term exponential function achieves the lowest error among all considered models.

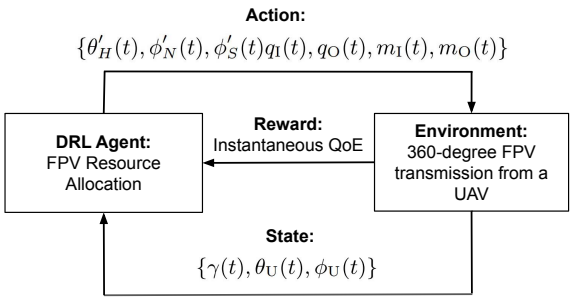

Fig. 6. Interaction of the deep reinforcement learning (DRL) agent with the environment for FPV adaptation.

TABLE II
Simulation Parameters

Parameter	Symbol	Value
Transmission frequency	f_{Fr}	28 GHz
Transmission bandwidth	B	400 MHz
UAV transmission power	P_{U}	0.1 Watts
Noise spectral density	N_o	$1.380649 \times 10.0^{-23}$
Horizontal limit of pilot's viewing angle (95% confidence bound)	θ_{H}	100°
Vertical South limit of pilot's viewing angle (95% confidence bound)	ϕ_{S}	70°
Vertical North limit of pilot's viewing angle (95% confidence bound)	ϕ_{N}	10°
Size of group of pictures	GOP	50
Weight assigned to frame quality within the pilot's central field of view	W_{C}	0.6
Weight assigned to frame quality within the pilot's peripheral field of view	W_{P}	0.35
Weight assigned to frame quality outside the pilot's field of view	W_{O}	0.05
Guarantee on constraint satisfaction	α	95%

B. FPV Adaptation Scenarios

The algorithms were evaluated for the simulation parameters listed in Table II, to provide a guarantee (α) of 95% on frame latency and probability of frame reception. A constant LDPC coding rate of $\frac{1}{3}$ was used. The horizontal viewport (θ'_{H}), north viewport (ϕ'_{N}), and south viewport (ϕ'_{S}) estimates were adapted in magnitude from 0° to 180° in steps of 30°. The modulation orders $(m_{\mathrm{I}}, m_{\mathrm{O}})$ were varied in a similar manner to 5G NR (2, 4, 16, 64, or 256), while the QPs $(q_{\mathrm{I}}, q_{\mathrm{O}})$ were varied from 10 to 50 in steps of 10. All urban and natural scenarios listed in Table I were evaluated. Two scenarios were considered - a hypothetical scenario in which the channel SNR was gradually increased from 0 to 40 dB over a time duration of 240 seconds. The SNR was increased by

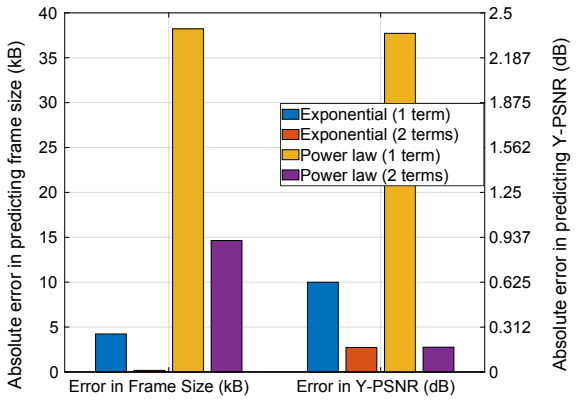

Fig. 7. Absolute error in predicting encoded frame Y-PSNR (measured in dB) and frame size (measured in kB) as a function of QP, for exponential and power law models, with one/two terms, for the aerial 360° video of Chicago.

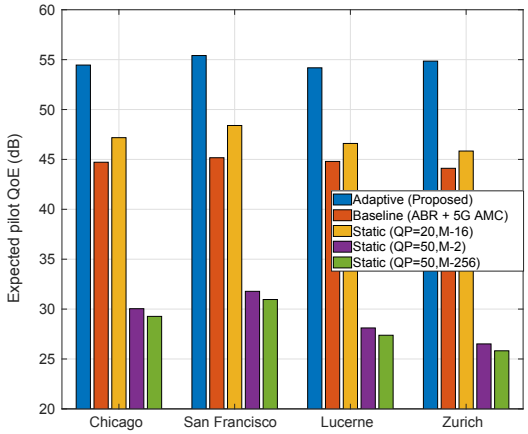

Fig. 8. Expected pilot QoE for: exhaustive resource allocation, static resource allocation approaches, and the baseline of adaptive bit-rate and 5G-NR adaptive modulation scheme, when UAV is flying over cities (urban environment).

1 dB every second. This scenario was designed to evaluate the algorithm performance over a comprehensive range of possible system inputs. The pilot viewing angle was varied as per (5) and (6). In the second scenario, we consider a more realistic variation in the channel SNR. The UAV was assumed to fly in a straight line from $(0, 0, 50)$ m to $(500, 500, 25)$ m at a velocity of 5 m/s, while being served wirelessly by mmWave BSs located on the ground, evenly distributed at intervals of 50 m along the x and y axes, at a height of 10 m.

C. Performance of Baseline and Static Resource Allocations

The expected value of the pilot QoE, is shown in Fig. 8 for UAV flights over cities and in Fig. 9 for UAV flights over nature. It can be seen that our proposed approach, represented by the blue bar, achieves the largest expected pilot QoE in all scenarios. Interestingly, the static resource allocation approach, which uses intermediate values for QP (20) and modulation order (16), outperforms the baseline method (5G-NR AMC and throughput-based ABR) in almost all scenarios. The delay

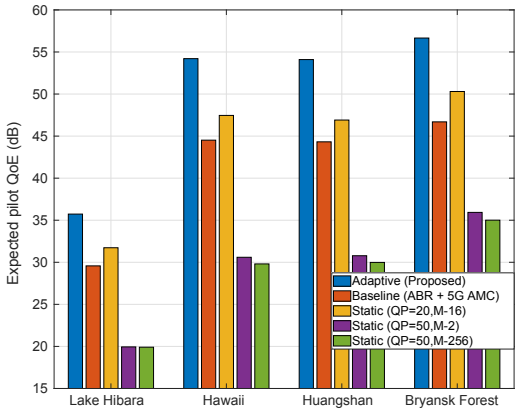

Fig. 9. Expected pilot QoE achieved by exhaustive resource allocation, static resource allocation approaches, and the baseline of adaptive bit-rate and 5G-NR adaptive modulation scheme, when the UAV is flying over nature.

in control of the ABR results in a performance loss. This implies that, while the principles of AMC are still applicable to aerial video transmissions, the specific AMC table designed for terrestrial communications can be improved upon for aerial video transmission. Over all considered videos, the proposed approach achieves a pilot QoE which is 9.46 dB (22%) higher than the baseline, and 6.89 dB (15.14%) higher than the closest static resource allocation. The CDF of the pilot QoE in the instantaneous QoE in the second scenario, where the UAV flies between two waypoints, is shown in Fig. 10, demonstrating the performance gains of our proposed approach.

D. Performance of Deep Reinforcement Learning

Here, we assess the performance of the deep RL framework for resource allocation. The DRL agent was implemented using Intel Coach [20], in both DDPG and DDQN architectures and evaluated for the videos of Chicago and Huangshan. The DRL agent requires intensive offline training, using simulations, to allow the neural network optimizer to all explore possible combinations of actions (optimization parameter values) in various states (channel SNR and pilot viewing directions). While this training process is time consuming, deploying the trained neural network online results in quick optimization, i.e. choosing the best parameter combinations for a given state requires only a single forward pass through the trained neural network network. The exhaustive search approach, on the other hand, does not require any offline training but results in slower online performance, since it has to search through all the possible parameter combinations. As shown in Fig. 11, the expected pilot QoE achieved by DDPG, averaged over the two scenarios, is just 2.074 dB lower than that achieved by the proposed adaptive approach. The DDQN architecture's performance is slightly worse than DDPG, achieving 2.57 dB less than the adaptive approach.

V. Conclusion

In this work, we theoretically modelled the transmission of 360° FPV from a UAV to the ground, and compared the performance of adaptive 360° transmission with a baseline

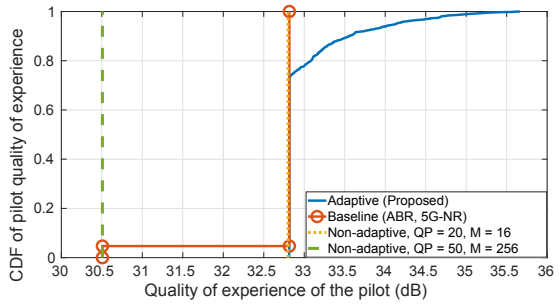

Fig. 10. CDF of the pilot QoE achieved by exhaustive resource allocation, static resource allocation approaches, and the baseline of adaptive bit-rate and 5G-NR adaptive modulation scheme, when the UAV flies in a straight line between two waypoints and is served by mmWave ground base stations.

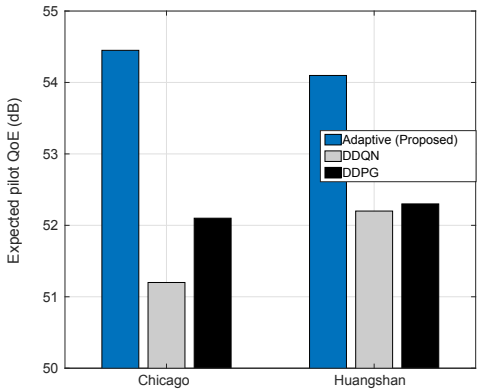

Fig. 11. Comparison of deep reinforcement learning (DRL) based FPV adaptation and resource allocation using exhaustive search, in terms of expected pilot QoE and standard deviation of pilot QoE.

approach using throughput-based ABR for QP selection and 5G-NR AMS for modulation order selection, to maximize the instantaneous QoE within the pilot's viewport. Non-adaptive approaches were also evaluated. We also formulated a DRL algorithm to optimize FPV with no prior knowledge of the environment. These approaches were evaluated on a wide dataset of videos of UAV flights over cities and nature and, in the considered scenarios, the adaptive approach was found to achieve 9.73 dB (21.77%) higher QoE than the baseline. The DRL-based algorithm achieves within 2.07 dB of the adaptive approach. We also utilized a two-term exponential function to model the variation in frame size and frame PSNR with QP. This model achieved lower prediction errors, compared to the single-term exponential and power law models generally used for rate-distortion characteristics. Our work can be used to improve UAV navigation applications, enabling the pilot to navigate the UAV with high immersion fidelity and increased responsiveness and safety.

References

[1] "Insta 360 Sphere VR," Nov. 2022. [Online]. Available: https://www.insta360.com/product/insta360-sphere

[2] R. Sacoto-Martins, J. Madeira, J. P. Matos-Carvalho, F. Azevedo, and L. M. Campos, "Multi-purpose Low Latency Streaming Using Unmanned Aerial Vehicles," in *2020 12th International Symposium on Communication Systems, Networks and Digital Signal Processing (CSNDSP)*, 2020, pp. 1–6.

[3] I.-S. Comşa, G.-M. Muntean, and R. Trestian, "An Innovative Machine-Learning-Based Scheduling Solution for Improving Live UHD Video Streaming Quality in Highly Dynamic Network Environments," *IEEE Transactions on Broadcasting*, vol. 67, no. 1, pp. 212–224, 2021.

[4] L. Zhang and J. Chakareski, "UAV-Assisted Edge Computing and Streaming for Wireless Virtual Reality: Analysis, Algorithm Design, and Performance Guarantees," *IEEE Transactions on Vehicular Technology*, vol. 71, no. 3, pp. 3267–3275, 2022.

[5] M. Khan, J. Chakareski, and S. Gupta, "F-FSO Dual-Path UAV Network for High Fidelity Multi-Viewpoint Scalable 360° Video Streaming," in *2020 IEEE 22nd International Workshop on Multimedia Signal Processing (MMSP)*. IEEE, 2020, pp. 1–6.

[6] J. Chakareski, "UAV-IoT for Next Generation Virtual Reality," *IEEE Transactions on Image Processing*, vol. 28, no. 12, pp. 5977–5990, 2019.

[7] ——, "Aerial UAV-IoT sensing for ubiquitous immersive communication and virtual human teleportation," in *Proc. INFOCOM Workshop on Communication and Networking Techniques for Contemporary Video*. Atlanta, GA, USA: IEEE, May 2017, pp. 718–723.

[8] ——, "Drone networks for virtual human teleportation," in *Proc. ACM MobiSys Workshop on Micro Aerial Vehicle Networks, Systems, and Applications (DroNet)*, Niaga Falls, NY, USA, Jun. 2017, pp. 21–26.

[9] L. Boban, L. Catania, D. Allegra, and M. Suznjevic, "Investigating the effect of region of interest coding on the qoe of fpv drone piloting under adverse network conditions," in *2023 17th International Conference on Telecommunications (ConTEL)*. IEEE, 2023, pp. 1–8.

[10] B. Chen, Z. Yan, H. Jin, and K. Nahrstedt, "Event-driven stitching for tile-based live 360 video streaming," in *Proceedings of the 10th ACM Multimedia Systems Conference*, ser. MMSys '19. New York, NY, USA: Association for Computing Machinery, 2019, p. 1–12. [Online]. Available: https://doi.org/10.1145/3304109.3306234

[11] X. Corbillon, G. Simon, A. Devlic, and J. Chakareski, "Viewport-adaptive navigable 360-degree video delivery," in *2017 IEEE International Conference on Communications (ICC)*, 2017, pp. 1–7.

[12] C. Madarasingha and K. Thilakarathna, "Vastile: Viewport adaptive scalable 360-degree video frame tiling," in *Proceedings of the 29th ACM International Conference on Multimedia*, ser. MM '21. New York, NY, USA: Association for Computing Machinery, 2021, p. 4555–4563. [Online]. Available: https://doi.org/10.1145/3474085.3475613

[13] Q. Zhu, M. Yao, F. Bai, X. Chen, W. Zhong, B. Hua, and X. Ye, "A general altitude-dependent path loss model for UAV-to-ground millimeter-wave communications," *Frontiers of Information Technology & Electronic Engineering*, vol. 22, no. 6, pp. 767–776, 2021.

[14] R. W. Verona, C. E. Rash, W. R. Holt, and J. K. Crosley, "Head movements during contour flight," ARMY AEROMEDICAL RESEARCH LAB FORT RUCKER AL, Tech. Rep., 1986.

[15] (2023, April) Airpano VR. [Online]. Available: https://www.airpano.com/

[16] J. Chakareski, R. Aksu, V. Swaminathan, and M. Zink, "Full UHD 360-Degree Video Dataset and Modeling of Rate-Distortion Characteristics and Head Movement Navigation," in *Proceedings of the 12th ACM Multimedia Systems Conference*, 2021, pp. 267–273.

[17] J. H. Bae, A. Abotabl, H.-P. Lin, K.-B. Song, and J. Lee, "An overview of channel coding for 5G NR cellular communications," *APSIPA Transactions on Signal and Information Processing*, vol. 8, p. e17, 2019.

[18] V. D. Bhise, *Ergonomics in the automotive design process*. CRC Press, 2011.

[19] L. Li, Q. Jiang, and W. Luo, "A Unified Non-CQI-based AMC Scheme for 5G NR Downlink and Uplink Transmissions," in *2021 IEEE 6th International Conference on Computer and Communication Systems (ICCCS)*. IEEE, 2021, pp. 881–886.

[20] (2023, April) Intel Reinforcement Learning Coach. [Online]. Available: https://intellabs.github.io/coach/

Appendix

The YouTube URLs of the aerial 360° videos we used are:

- Chicago: https://www.youtube.com/watch?v=IfQ7Bjg823M
- Lucerne: https://www.youtube.com/watch?v=uzk0q5eoBY0
- San Francisco: https://www.youtube.com/watch?v=tjQGnXBn1WA
- Zurich: https://www.youtube.com/watch?v=P3jyeihhCWk
- Bryansk Forest: https://www.youtube.com/watch?v=dKVdgnK9Zsw
- Hawaii: https://www.youtube.com/watch?v=yagTn5Cud_I
- Huangshan: https://www.youtube.com/watch?v=0YwaAgB_-nw.
- Lake Hibara: https://www.youtube.com/watch?v=VUVDXSJqYbM